Available online at www.sciencedirect.com
SCIENCE DIRECT®
Icarus 181 (2006) 527–544
ICARUS
www.elsevier.com/locate/icarus

Predictions of the electrical conductivity and charging of the aerosols in Titan's atmosphere

W.J. Borucki [a,*], R.C. Whitten [b], E.L.O. Bakes [b], E. Barth [c], S. Tripathi [d]

[a] *NASA Ames Research Center, M.S. 244-30, Moffett Field, CA 94035, USA*
[b] *SETI Institute, Mountain View, CA 94043, USA*
[c] *Southwest Research Institute, San Antonio, TX 78228, USA*
[d] *Indian Institute of Technology, Kanpur 208016, India*

Received 23 December 2004; revised 4 October 2005

Available online 9 February 2006

Abstract

The electrical conductivity and electrical charge on the aerosols in atmosphere of Titan are computed for altitudes between 0 and 400 km. Ionization of methane and nitrogen due to galactic cosmic rays (GCR) is important at night where these ions are converted to ion clusters such as $CH_5^+CH_4$, $C_7H_7^+$, $C_4H_7^+$, and $H_4C_7N^+$. The ubiquitous aerosols observed also play an important role in determining the charge distribution in the atmosphere. Because polycyclic aromatic hydrocarbons (PAHs) are expected in Titan's atmosphere and have been observed in the laboratory and found to be electrophilic, we consider the formation of negative ions. During the night, the very smallest molecular complexes accept free electrons to form negative ions. This results in a large reduction of the electron abundance both in the region between 150 and 350 km over that predicted when such aerosols are not considered. During the day time, ionization by photoemission from aerosols irradiated by solar ultraviolet (UV) radiation overwhelms the GCR-produced ionization. The presence of hydrocarbon and nitrile minor constituents substantially reduces the UV flux in the wavelength band from the cutoff of CH_4 at 155 to 200 nm. These aerosols have such a low ionization potential that the bulk of the solar radiation at longer wavelengths is energetic enough to produce a photoionization rate sufficient to create an ionosphere even without galactic cosmic ray (GCR) bombardment. At altitudes below 60 km, the electron and positive ion abundances are influenced by the three-body recombination of ions and electrons. The addition of this reaction significantly reduces the predicted electron abundance over that previously predicted. Our calculations for the dayside show that the peaks of the charge distributions move to larger values as the altitude increases. This variation is the result of the increased UV flux present at the highest altitudes. Clearly, the situation is quite different than that for the night where the peak of the distribution for a particular size is nearly constant with altitude when negative ions are not present. The presence of very small aerosol particles (embryos) may cause the peak of the distribution to decrease from about 8 negative charges to as little as one negative charge or even zero charge. This dependence on altitude will require models of the aerosol formation to change their algorithms to better represent the effect of charged aerosols as a function of altitude. In particular, the charge state will be much higher than previously predicted and it will not be constant with altitude during the day time. Charging of aerosol particles, whether on the dayside or nightside, has a major influence on both the electron abundance and electrical conductivity. The predicted conductivities are within the measurement range of the HASI PWA instrument over most but not all, of the altitude range sampled.
© 2005 Elsevier Inc. All rights reserved.

Keywords: Titan; Ionospheres; Radiation chemistry; Photochemistry

1. Introduction

The charging of the aerosols in Titan's atmosphere is important because the predicted electron densities and thus the electrical conductivity in the lower atmosphere are reduced and aerosol coagulation is inhibited (Cabane et al., 1992; Toon et al., 1992). The latter effect favors larger concentrations of small

* Corresponding author.
E-mail address: william.j.borucki@nasa.gov (W.J. Borucki).

0019-1035/$ – see front matter © 2005 Elsevier Inc. All rights reserved.
doi:10.1016/j.icarus.2005.10.030

particles and fewer large particles. These particles in turn affect the vertical deposition of solar energy and thus the structure of the atmosphere.

In an early paper, Capone et al. (1980) computed the expected electron and ion abundances as a function of altitude produced by the GCR. The substantial effects of aerosols on these abundances was first recognized by Borucki et al. (1987). Because aerosol characteristics were poorly known at that time, especially with respect to their variation with altitude, they conducted parametric studies of the effect of both mono- and polydisperse aerosols on the ion and electron abundances. They also assumed that no electrophilic species were likely to be present in sufficient abundance to significantly attach the electrons and that photoelectron emission by the aerosol particles was not significant. Even with increased recombination rates caused by the aerosols, their calculations concluded that the atmosphere would be orders of magnitude more conductive than the terrestrial atmosphere.

In Borucki et al. (1987), ionization by galactic cosmic rays was computed by adapting to Titan models developed by O'Brien (1970, 1971, 1972). Since the model atmosphere used there was quite close to the more recent one used in this paper, we used the ionization rate profile of Borucki et al. (1987). The earlier paper employed the charged particle transport properties at low altitudes (diffusion) developed by Hodges (1969), used a continuum distribution of charges rather than an integer charge model as developed by Parthasarathty (1976), and neglected three-body electron–ion recombination at low altitudes. All of these limitations have been removed in the computations reported here.

Jensen and Thomas (1991) constructed a model for computing the attachment of electrons and ions to polar mesospheric clouds on Earth. Since atmospheric density is too small for diffusion to be significant in the mesosphere, they treated effusion only. For this purpose they included the charge distribution algorithm of Parthasarathty (1976) [see Eq. (15) below] and the image charge method developed by Natanson (1960). [Also see Landau et al. (1984).] We have adapted the approach of Jensen and Thomas (1991) to the effusion regime on Titan.

Lara et al. (1999) pointed out that a carbon to nitrogen ratio as low as 2:1 could be justified in the formation of Titan hazes thereby bringing model predictions of HCN into better agreement with observations. A model study by Molina-Cuberos et al. (1999a, 1999b) predicted that hydrocarbon cations such as $CH_5^+CH_4$ rather than nitrogenated cations assumed by Borucki et al. (1987) would dominate at altitudes below 270 km. They also showed that the peak in the electron abundance of 2150 cm^{-3} would occur at 90 km and vary by 10% depending on the solar cycle. However, they did not include the effect of aerosols. Studies by Lebonnois et al. (2002) and Wilson and Atreya (2004) suggest the production of poly-aromatic hydrocarbons (PAH) as the most promising candidate for the composition of the Titan haze layer. Bakes et al. (2002) noted that the monomers and polymers of PAH could be very abundant in Titan's atmosphere and that these molecular complexes would be electrophilic. Although they would be lost by thermal coagulation before reaching altitudes below 120 km, they could serve as negative ions above that altitude and thereby attach electrons and reduce their abundance. Precursors (benzene) to the monomers needed for the formation of PAHs have been observed in Titan's atmosphere (Coustenis et al., 2003). Consequently, it appears appropriate to consider their effects on the ion and electron abundances and the atmospheric conductivity.

In this paper, the conductivity of the atmosphere and electrical charge on the aerosols in the altitude range from 0 to 400 km are estimated from steady-state calculations based on the ionization due to the absorption of high-energy particles by atmospheric gases and solar UV radiation by aerosol particles followed by the recombination of the ions and electrons.

In the night time atmosphere of Titan, the attachment of electrons to the aerosol substantially reduces the electron abundance and the atmospheric conductivity. On the dayside, solar ultraviolet radiation impinging on the aerosol particles causes emission of electrons, leaving the particles with positive charge and greatly increasing the atmospheric conductivity. Thus the ubiquity of the aerosols substantially changes the planetary conductivity profile from what it would be if they were not present. Although spacecraft measurements clearly show the presence of these aerosols, the measurements do not furnish enough information on the number and size distributions as a function of altitude to permit direct calculations of the effects of the aerosols. Consequently, our calculations use theoretical predictions of the aerosol parameters that are consistent with the spacecraft measurements.

Our model is based on that described by Borucki et al. (1987) with several modifications. In particular it now includes:

(1) a more accurate method of calculating the total aerosol charge and charge distributions,
(2) a three-body reaction rate for the recombination of positive ions with electrons,
(3) ionization of molecules and aerosols from both GCR and solar UV flux,
(4) a range of aerosols sized from 3 Å to 0.3 μm based on the Toon et al. (1992) Titan aerosol model,
(5) day time conditions are considered,
(6) the effects of Raleigh scattering, absorption and scattering by aerosols, and absorption by minor constituents,
(7) photoemission charging of aerosols.

The model is fully interactive with respect to the formation and recombination of electrons, charged ions, and aerosols and computes self-consistent distributions of integral charges on all particle sizes.

This paper is organized into the following sections: atmospheric environment, formation of the lower ionosphere, aerosol distribution, computation of aerosol charging, effect of photoionization on aerosol charging, and results. In the Results section, discussions are provided for atmospheric conductivity and its comparison with the measurement capability of the Huygens Atmospheric Structure Instrument (HASI).

2. Atmospheric environment

To calculate the conductivity of the atmosphere it is necessary to choose a standard atmosphere. Table 1 presents values of the temperature, pressure, and number density as a function of altitude taken from recommended model atmosphere described by Yelle et al. (1996). This model is consistent with both direct measurements of thermal profiles and composition and with theoretical profiles based on hydrostatic equilibrium. The temperature and pressure at the base of the atmosphere are 93.9 K and 1.44 bar, respectively. Below 600 km, the atmosphere is well mixed and the atmospheric composition is taken to be constant with 95% N_2, 3% CH_4, and 2% Ar. The actual abundance of Ar and methane are poorly constrained. In particular, Lara et al. (1996) find that a methane abundance of 1.5% to 2% provides a better fit to the minor species abundances. Because modest variations in the assumed composition and temperature profile cause only minor variations in the results reported here, the model of Yelle et al. (1996) is adopted without modification. Much more significant uncertainties are caused by the abundance and identities of the minor species present and by the aerosol properties.

3. Formation of the lower ionosphere

3.1. Ionization due to GCR

Both galactic cosmic rays (GCR) and photoionization of the aerosols cause significant ionization. (Electron precipitation is important above 700 km, but is usually a minor contributor below 400 km.) The importance of GCR in the context of the present study is two-fold. First, since the intensity of the solar EUV radiation decreases as the square of the distance from the Sun, GCR-induced ionization assumes greater relative importance in the atmospheres of the outer planets and satellites. In addition, the GCR-induced electromagnetic and particle cascade will penetrate to relatively large depth (i.e., high pressures) in the extended, massive atmosphere of Titan.

Table 1
Model atmosphere and ion production rate from GCR

Altitude (km)	Pressure (bar)	Temp. (K)	Mass density (kg/m^3)	Ion prod. rate (pairs/cc/s)	$[N_2 + CH_4]$ (#/m^3)
0	1.46E+00	93.28	5.44	0.260	1.16×10^{26}
20	4.84E−01	76.43	2.16	0.350	4.68×10^{25}
40	1.41E−01	70.66	0.673	0.450	1.46×10^{25}
60	4.19E−02	76.87	0.183	1.000	3.96×10^{24}
80	1.77E−02	123.61	4.79E−01	10.02	1.40×10^{24}
100	9.43E−03	142.06	2.22E−01	14.000	4.80×10^{23}
120	5.35E−03	151.00	1.18E−01	8.310	2.56×10^{23}
140	3.15E−03	158.55	6.65E−01	4.95	1.44×10^{23}
160	1.91E−03	163.77	3.90E−01	2.93	8.43×10^{22}
180	1.18E−03	167.30	2.36E−01	1.69	5.10×10^{22}
200	7.42E−04	170.48	1.46E−01	1.02	3.11×10^{22}
220	4.73E−04	172.58	9.13E−02	0.47	2.88×10^{22}
240	3.05E−04	175.42	5.82E−02	0.22	1.24×10^{22}
260	1.99E−04	177.02	3.76E−02	0.118	1.03×10^{22}
280	1.31E−04	177.97	2.46E−02	0.076	6.74×10^{21}
300	8.70E−05	178.19	1.63E−02	0.049	3.58×10^{21}
320	5.80E−05	177.63	1.09E−02	0.035	2.39×10^{21}
340	3.88E−05	176.21	7.36E−03	0.024	1.61×10^{21}
360	2.60E−05	173.85	5.00E−03	0.019	1.10×10^{21}
380	1.74E−05	170.60	3.41E−03	0.018	7.48×10^{20}
400	1.16E−05	166.61	2.33E−03	0.017	5.11×10^{20}

Since the energies of the cosmic rays incident upon a planetary atmosphere span many orders of magnitude (with a non-negligible fraction of the total energy carried by multi-TeV particles), a number of processes must be considered in order to describe the distribution of the cosmic-ray energy throughout an atmosphere. Collisions of the primary cosmic rays (mostly protons with a small fraction of heavier ions) produce a cascade of many particles including secondary protons, neutrons, pions, electrons, and gamma rays. These in turn undergo further cascading collisions with the atmosphere. In addition, the pions decay into either gamma rays or muons and neutrinos and the muons eventually decay into electrons and neutrinos. The energy deposition in the atmosphere is then calculated by folding the charged particle fluxes (except electrons) with the stopping power for the various particles and the various atmospheric constituents. We do not attempt to calculate in detail the electromagnetic cascade of the (relatively low energy) electrons and gammas but assume that their total energy is deposited at the point of production. Since the interaction of neutrinos with matter is so weak, we assume that the energy carried by the neutrinos is transported out of the atmosphere.

The ionization rates due to bombardment of the atmosphere by galactic cosmic rays were taken from those published earlier by Borucki et al. (1987) and are similar to those of Molina-Cuberos et al. (1999a). The mathematical development of our approach, the approximations employed, and the physical input used have been described in detail elsewhere (Borucki et al., 1987). The ionization model was an adaptation to Titan of a model developed for Earth by O'Brien (1971, 1972, 1975a, 1975b).

The contribution to ionization from precipitating particles from the saturnian magnetosphere (Krimingis et al., 1983; Vogt et al., 1981) was included as described in (Borucki et al., 1987). The small contribution from precipitating electrons above 350 km is noticeable as break in the decreasing ionization rate with altitude (see Fig. 1). Ionization by precipitating protons is negligible in the atmosphere below 350 km.

When Titan is outside the magnetosphere of Saturn, only galactic cosmic rays and the low-energy particle of the solar wind are present. At such times the ionization from precipitating electrons will be absent. The slowly varying (with altitude) "tail" below 60 km is the result of ionization by muons.

3.2. Calculation of the ion- and electron-density profiles

During the night, galactic cosmic rays are the main ionization source in the lower atmosphere of Titan below 400 km, as explained above, and ionize the neutral constituents (mainly N_2, CH_4, Ar, H_2, and CO), producing N_2^+, N^+, Ar^+, CH_4^+, CH_3^+, CH_2^+, H_2^+, H^+, CO^+, and electrons. Fast reactions with the neutrals rapidly convert these ions into secondary ions and ion

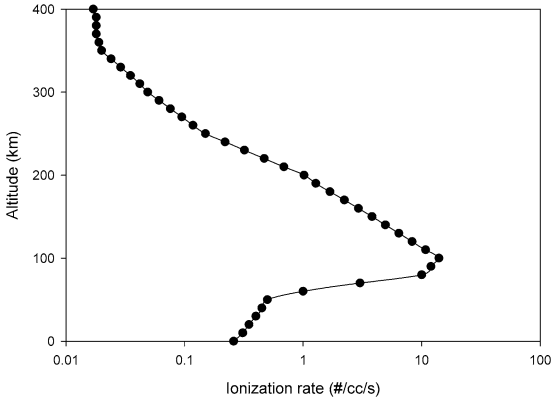

Fig. 1. Ionization rate from galactic cosmic rays and from precipitating electrons as a function of altitude.

clusters. Studies on stratospheric conductivity on Earth (where cosmic rays are also the main ionization source at large atmospheric depths) suggest that small positive and negative ions (molecular cluster ions) provide the main contribution to the stratospheric conductivity (Hu and Holzworth, 1996). These cluster ions are removed by their recombination with ions of opposite charge and by attachment to aerosol particles.

3.2.1. *Formation of positive secondary ions and positive ion clusters*

The initial ionization of methane and nitrogen is followed by a series of reactions that eventually produce massive positive ions (30 to 102 amu) having recombination coefficients and mobilities that are different from those of N_2^+ and CH_4^+. The formation of large ions is discussed at length in Appendix A. For the calculations presented here, the identity of the ions is much less important than their mass which largely determines their mobility and recombination rate.

3.2.2. *Formation of negative secondary ions and negative ion clusters*

In Borucki et al. (1987), the ion concentrations and conductivity in the night time Titan atmosphere were first calculated using only gas kinetic charge balance equations. These showed that the lack of electrophilic species led to a very high electron concentration compared to those in the terrestrial and venusian atmospheres. When the electron attachment to aerosols was also considered, modest decreases in the electron concentration and conductivity were predicted. Nevertheless, the large abundance of free electrons was still high enough to produce a conductivity about 300 times larger than found in the Earth's atmosphere at similar column densities. Later calculations performed by Lara et al. (1996) predict the presence of electrophilic species such as H, CH_3, and C_3H_2 in the lower atmosphere. However, the concentrations of these electrophilic species are predicted to be too low to affect the abundance of electrons.

Molina-Cuberos et al. (2000) calculated the ion concentration in the lower 70-km of Titan atmosphere based on a parametric study assuming various levels of a hypothetical electrophilic species. They found that a mixing ratio of electrophilic species of at least 10^{-14} is required near the surface to produce an abundance of negative ions sufficiently large to reduce the predicted electron abundance. With increasing altitude, it is necessary to have even higher concentrations of such species to obtain an appreciable number of anions. Their results are in good agreement with those of Borucki et al. (1987). Because concentrations of molecular ions formed from H, CH_3, and C_3H_2 are expected to be much lower, they will not be considered further.

Recently, it has been postulated that the ubiquitous aerosols found in the atmosphere might be composed of aggregated clusters of polycyclic aromatic hydrocarbons (PAHs) (Bakes et al., 2002). These aerosols and the clusters from which they form, are likely to be present over a large range of sizes. The smallest clusters could play the role of negative ions in that they are of sufficiently low mass to have a significant mobility when charged. Furthermore, PAHs are known to be electrophilic (Bakes and Tielens, 1994, 1998) and thereby can potentially reduce the otherwise large abundance of free electrons. For these reasons we include them in our calculations of the charge distribution and conductivity of the Titan atmosphere.

3.2.3. *Calculation of the mobilities and diffusivities*

The positive- and negative-ion mobilities (K_+ and K_-, respectively) were interpolated from the mobility versus ion-mass dispersion curve for molecular ions in nitrogen given in Meyerott et al. (1980) and Kilpatric (1971) in which we included the reduced-mass correction. These values are similar to those determined by Rosen et al. (1982) for ions in the Earth's atmosphere between 5 and 30 km altitude.

The electron mobility K_e for each altitude is calculated from the momentum transfer collision frequency of electrons in nitrogen. The values are taken from the experimental measurements of Ramanan and Freeman (1990) for elastic collisions at low temperatures. The diffusion coefficients are then obtained from the mobility using the Einstein relation $D^j = K_j kT/e$ (McDaniel and Mason, 1973), where k is the Boltzmann constant ($j = 1, 2, 3$ for electron, positive ion, and negative ion, respectively).

Table 2 presents some calculated values for the ion and electron mobilities and diffusivities as a function of altitude. The much higher values of the electron mobility and diffusivity cause the aerosols to be charged negatively at all altitudes during the night time when no solar flux is available to photoionize the aerosols and ions.

4. Aerosol distributions

Spacecraft observations have shown that aerosols are abundant in the Titan atmosphere. When the presence of aerosols is considered, our calculations show that the aerosol size and number density strongly affect the predicted values of the electron concentration.

Size information is derived from the data obtained from the Voyager photopolarimeter observations (West et al., 1983). Voyager high-phase-angle images (Rages et al., 1983) and photometry and polarimetry measurements from Pioneer 11 (Tomasko and Smith, 1982). Analysis of Voyager 2 images by

Table 2
Calculated values of the mobilities and diffusivities of the ion clusters and electrons

Altitude (km)	Positive ion mobility ($m^2/v/s$)	Electron mobility ($m^2/v/s$)	Negative ion mobility ($m^2/v/s$)*	Positive ion diffusivity (m^2/s)	Electron diffusivity (m^2/s)	Negative ion diffusivity (m^2/s)*
0	6.180E−5	8.300E−1		4.970E−7	6.670E−3	
10	9.440E−5	1.410E+0		6.760E−7	1.010E−2	
20	1.560E−4	2.520E+0		1.030E−6	1.660E−2	
30	2.730E−4	4.650E+0		1.700E−6	2.900E−2	
40	4.990E−4	8.690E+0		3.040E−6	5.300E−2	
50	9.380E−4	1.620E+1		5.770E−6	9.960E−2	
60	1.840E−3	2.950E+1		1.220E−5	1.960E−1	
70	4.060E−3	4.930E+1		3.640E−5	4.420E−1	
80	7.010E−3	7.250E+1		7.480E−5	7.730E−1	
90	0.011	1.010E+2		1.230E−4	1.180E+0	
100	0.015	1.380E+2	8.220E−3	1.850E−4	1.690E+0	1.010E−4
110	0.017	1.850E+2	0.019	2.110E−4	2.340E+0	2.370E−4
120	0.019	2.450E+2	0.018	2.500E−4	3.180E+0	2.340E−4
130	0.026	3.190E+2	0.028	3.490E−4	4.310E+0	3.790E−4
140	0.034	4.150E+2	0.034	4.660E−4	5.670E+0	4.690E−4
150	0.045	5.350E+2	0.047	6.260E−4	7.470E+0	6.520E−4
160	0.070	6.860E+2	0.066	9.930E−4	9.700E+0	9.310E−4
170	0.090	8.750E+2	0.081	1.290E−3	1.250E+1	1.150E−3
180	0.116	1.110E+3	0.107	1.680E−3	1.600E+1	1.540E−3
190	0.148	1.410E+3	0.134	2.160E−3	2.050E+1	1.950E−3
200	0.188	1.770E+3	0.171	2.760E−3	2.600E+1	2.520E−3
210	0.238	2.230E+3	0.216	3.530E−3	3.300E+1	3.210E−3
220	0.300	2.780E+3	0.273	4.480E−3	4.160E+1	4.080E−3

* The abundance of negative ions is negligible below 100 km.

Rages and Pollack (1983) indicate that between 220 and 350 km the aerosol particles have radii near 0.3 μm and have number densities that range from about 0.2 particles/cc at 350 km to 2 particles/cc near 220 km.

While we have assumed the particles to be spherical because of the lack of knowledge of their true shapes, the shapes could be fractal (Cabane et al., 1993; Rannou et al., 1995, 1997). Such shapes cause substantial increases the surface area for a given mass loading, especially for small particles. The increased surface area will cause somewhat larger photoelectron emission rates and larger electron and ion capture rates by the particles. On the dayside these two effects tend to cancel each other, diminishing the fractal effect; such cancellation would not, of course, occur on the nightside. However, in view of other rather large uncertainties in the cloud properties, the fractal nature of the particles is not expected to cause unacceptable error in our results.

The spacecraft data provide some constraints on the actual aerosol distribution in that the optical depth between 350 and 220 km and the total optical depth can be estimated. However, particles smaller than 0.1 μm do not scatter light efficiently enough to be detected on spacecraft images. Because spacecraft measurements have not adequately determined the aerosol size distributions, shapes, abundances, nor their variation with altitude, the results of the theoretical model by Toon et al. (1992) are used to estimate these quantities.

This model simulates the physics of production, growth and transport of the aerosol particles and is consistent with the spacecraft measurements. It is described in Appendix B. The particle size and number density data obtained from Barth and Toon (2003) were contained in 31 size bins. To facilitate the electrical charging computations the largest 31 bins were sorted into 6 size bins using the method discussed in Section 5.2.

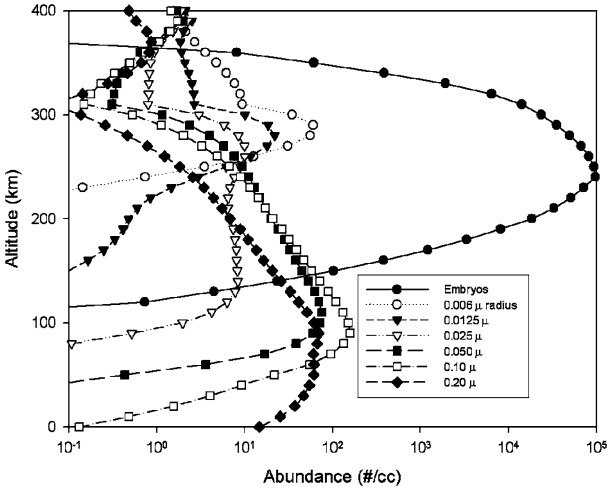

Fig. 2. Aerosol abundances versus altitude for wide bins.

Fig. 2 shows the model aerosol size distributions as a function of altitude for several size bins. As expected, the smaller sizes are prevalent at the higher altitudes while the larger sizes are found mainly at lower altitudes. Maxima in abundances for the three largest size bins occur in the 50 to 120 km altitude range; i.e., at altitudes that the Huygens Atmosphere Structure Instrument (HASI) will sample.

Because the loss rates of positive ions and electrons to aerosol particles are a strong function of the aerosol abundance

and size, the aerosol model employed here uses a detailed size distribution that varies with altitude. Further, the distribution of charge on each particle size is calculated. At each altitude, the charge distribution of each particle size is a function of those on all other sizes as well as the abundance of ions and electrons. Hence a simultaneous set of nonlinear equations must be solved.

5. Computation of aerosol charging

Our model of the electrical charging of the aerosol particles is based on the work of Natanson (1960), Parthasarathty (1976), and especially Jensen and Thomas (1991, hereafter called JT). Since the theory is presented in considerable detail by JT, the reader is referred to their paper in the interest of saving space.

The aerosols are assumed to be composed of polycyclic aromatic hydrocarbons, The composition is important because of its low ionization potential and because such material is electrophilic. The lowest mass aerosols (containing the order of 10 to 30 carbon atoms and a radius $\sim 3 \times 10^{-4}$ μm) are mobile with respect to the atmosphere and will henceforth be referred to as "embryos." They are found in sufficient abundance to affect the atmospheric conductivity above 150 km where they become charged and form negative ions. Further, the low ionization potential of this material promotes the production of free electrons during the day time.

5.1. Numerical procedures

The charge balance equations are solved by means of an iterative procedure briefly described below during which the distribution of charge on the aerosols is simultaneously computed. At high altitude (i.e., above 300 km) in the Earth's ionosphere, ambipolar diffusion of ions and electrons must be included in the charge balance equations. However for Titan, the atmospheric density at 400 km altitude corresponds to about 90 km on Earth, which is far below the altitude where ambipolar diffusion becomes important. Moreover, we estimated the recombination time for electrons and ions and found that it is much less than 1 s whereas the time for an electron–ion pair to diffuse 1 m is about 10^4 s. Hence vertical transport does not significantly affect our results.

5.1.1. Solution of the charge balance equations

The rate equations for the electron, positive ion and negative embryo[1] densities at each altitude are:

$$\frac{dn_e}{dt} = Q + \sum_{i,p} \zeta_{a,p} N_{i,p} + \zeta_- n_- + \zeta^{\text{emb}} n_{\text{emb}} - \{\alpha_1 + \alpha_2([N_2] + [CH_4])\} n_e (n_+ + n_{+m}) - d_e n_e - \beta n_{\text{emb}} n_e, \quad (1)$$

$$\frac{dn_+}{dt} = Q + \zeta^{\text{emb}} n_{\text{emb}} - \{\alpha_1 + \alpha_2([N_2] + [CH_4])\} n_e n_+ - \alpha_3 n_+ n_- - d_+ n_+, \quad (2)$$

$$\frac{dn_-}{dt} = \beta n_{\text{emb}} n_e - \alpha_3 n_+ n_- - d_- n_- - \zeta_- n_-, \quad (3)$$

$$\frac{dn_{+m}}{dt} = \zeta^{\text{emb}} n_{\text{emb}} - \{\alpha_1 + \alpha_2([N_2 + CH_4])\} n_{+m} n_e. \quad (4)$$

It is assumed that embryos can be charged negatively by collision and can lose this electron by photoejection. Neutral embryos can also eject electrons as a result of absorption of solar UV radiation and this process is included on the dayside. Here recombination with electrons is the governing loss process for which we use the same value as that for electron dissociative recombination with molecular positive ions.

The requirement that every volume of space be electrically neutral imposes the condition

$$zp + n_{+m} + n_+ - n_- - n_e = 0, \quad (5)$$

$$zp = \sum_{i,p} p N_{i,p}. \quad (6)$$

Conservation of the number of embryos requires that

$$n_T = n_{+m} + n_- + n_{\text{emb}}, \quad (7)$$

where:

Q	is the molecular ionization rate ($m^{-3}\ s^{-1}$) due to energetic particle radiation
α_1	is the electron–positive ion dissociative recombination coefficient
α_2	is the pressure-dependent electron–positive ion three-body recombination coefficient ($m^3\ s^{-1}$)
α_3	is the negative ion–positive ion recombination coefficient ($4.0 \times 10^{-13}\ m^3\ s^{-1}$); these recombination coefficients are typically smaller than α_1 (for example, see Holland et al., 1977)
β	is the attachment coefficient of electrons to embryos ($6.0 \times 10^{-12}\ m^3\ s^{-1}$; Bakes and Tielens, 1994)
d_e	is the combined diffusion/effusion rate of electrons to aerosol particles (s^{-1})
d_+	is the combined diffusion/effusion rate of positive ions (s^{-1}) to aerosol particles
d_-	is the combined diffusion/effusion rate of negative ions (s^{-1}) to aerosol particles
ζ^-	is the photoejection rate of electrons from negative ions (s^{-1})
$\zeta^a_{i,p}$	is the photoejection rate of electrons from aerosols in size bin "i" and with charge p (s^{-1})
ζ^{emb}	is the photoejection rate of electrons from embryos (s^{-1})
n_e	is electron density (m^{-3})
n_+	is positive ion density (m^{-3})
n_-	is negative ion density (m^{-3})
n_T	is total number of embryos (m^{-3})
n_{emb}	is neutral embryo density (m^{-3})

[1] Henceforth negatively charged embryos will be referred to as "negative ions." See the discussion in a later section.

n_{+m} is number density of positively charged embryos (m^{-3})
N is total number density of aerosols (m^{-3})
$N_{i,p}$ is number density of aerosols in size bin "i" and with charge state "p"
zp is the total charge on the aerosols with sign (m^{-3})

The assumption of steady state is justified because the recombination "time constants" for recombination of electrons with positive ions and capture of electrons by positively charged aerosol particles is less than 100 and 1 s respectively for both day- and nightsides. Thus, the production and loss terms for electrons, positive ions, and negative ions are, respectively,

$$Q + \sum_{i,p} \zeta^a_{i,p} N_{i,p} + \zeta^- n_- + \zeta^{\text{emb}} n_{\text{emb}} = \{\alpha_1 + \alpha_2([N_2] + [CH_4])\}(n_{\text{emb}} + n_+)n_e + d_e n_e + \beta n_{\text{emb}} n_e, \quad (8)$$

$$Q + \zeta^{\text{emb}} n_{\text{emb}} = \{\alpha_1 + \alpha_2([N_2] + [CH_4])\} n_e (n_+ + n_{+m}) + d_+ n_+ + \alpha_3 n_- n_+, \quad (9)$$

$$\beta n_{\text{emb}} n_e = \alpha_3 n_- n_+ + d_- n_- + \zeta^- n_-. \quad (10)$$

Numerical routines are used to solve the set of equations at 10 km altitude intervals. The method outlined in Jensen and Thomas (1991) was used to estimate the initial estimates of the unknowns.

The mathematical routine used to solve the coupled set of Eqs. (11)–(13) is based on a multi-dimensional minimization of a function of the dependent variables, positive ion density, electron density, total charge on the aerosol particles; and the density of the charged embryos (if present). The downhill simplex method of Nelder and Mead (1965) requires only the evaluation of the function to be minimized and not the derivative of the function

$$f_1 = Q + \sum_{i,p} \zeta_{a,p} N_{i,p} + \zeta_- n_- + \zeta^{\text{emb}} n_{\text{emb}} - \{\alpha_1 + \alpha_2([N_2] + [CH_4])\} n_e (n_+ + n_{+m}) - d_e n_e - \beta n_{\text{emb}} n_e, \quad (11)$$

$$f_2 = \beta n_{\text{emb}} n_e - \alpha_3 n_- n_+ - d_- n_- - \zeta^- n_-, \quad (12)$$

$$f_3 = zp + n_+ + n_{+m} - n_e - n_-. \quad (13)$$

To solve these equations, initial estimates for n_+, n_e, n_-, n_{+m}, and the $N_{i,p}$ are required. To obtain these, n_- and n_{+m} are set to zero, and the charge on the aerosol particles set to arbitrary values within the range of likely values.

Then the initial values of the positive ion and electron densities are computed from Eqs. (4) and (7). These starting values are then inserted into the function to be minimized as the first step in the iterative process. The iterative process is continued, using the charge cascade expression Eq. (15) until the value of f in Eq. (14) is less than some very small value, typically 10^{-10},

$$f^2 = (f_1)^2 + (f_3)^2. \quad (14a)$$

For computations of the nightside it was necessary to include Eq. (12), replacing Eq. (14a) by

$$f^2 = (f_1)^2 + (f_2)^2 + (f_3)^2. \quad (14b)$$

At each step in the iterative cycle, the negatively and positively charged embryos are estimated from Eq. (6) (with the time derivative set to zero).

To solve for the abundance of the positive embryos, Eq. (4) is used to solve for n_m^+ and the equations for n_m^- and n_m^+ are iterated within the function f to be minimized. This procedure is justified on the dayside, but not on the nightside when Eq. (14b) must be used, because the abundances of n_m^- and n_m^+ are much smaller than that of n_e. In short, Eq. (10) is treated as a perturbation of Eqs. (8) and (9). A similar procedure is used for the computation of n_m^+. At altitudes below 150 km, negative ions are unimportant and are excluded from the computations and minimization of f in Eq. (14) yields positive ion, electron and charged aerosol densities with computed errors less then one percent.

Because of this iterative process only two equations are required; electron and ion densities from the preceding step are used in function f to compute the charge on the aerosol particles in the current step with the result that such charge is not independent of the ion and electron number densities.

The computations become more complicated when negatively and positively charged embryos are included. The minimization routine described above does not work very well for more than two continuity equations. Hence we employ Eq. (10) to partition charge between the electrons and the negative ions by means of a short iterative procedure within the function f. We use a similar procedure to partition charge between positively charged molecular ions and positively charged embryos. The minimization subroutine uses the downhill simplex method cited above for which the Fortran code is provided in Press et al. (1986).

5.1.2. *Calculation of the charge distribution on the aerosols*

The reduction of ions and electrons due to the presence of the aerosols is calculated by the method described in JT:

$$N_{i,p}\zeta^a_{i,p} + N_{i,p}\nu_p^{i,+} n_+ + N_{i,p}\nu_p^{i,e} n_e + N_{i,p}\nu_p^{i,-} n_- = N_{i,p+1}\nu_{p+1}^{i,e} n_e + N_{i,p+1}\nu_{p+1}^{i,-} n_- + N_{i,p-1}\nu_{p-1}^{i,+} n_+ + N_{i,p-1}\zeta^a_{i,p-1}, \quad (15)$$

where:

$N_{i,p}$ is the fractional concentration of aerosol particles with size "i," and charge "p"
$\nu_p^{i,e}$ is the capture rate coefficient for electrons by particles with charge p ($m^3\ s^{-1}$)
$\nu_p^{i,+}$ is the capture rate coefficient for positive ions by aerosols with charge p ($m^3\ s^{-1}$)
$\nu_p^{i,-}$ is the capture rate coefficient of negative ions to aerosols with charge p ($m^3\ s^{-1}$)

The "ν's" are dependent upon the aerosol particle radius (size mode) as well as charge. Evaluation of Eq. (15) is performed by first solving Eqs. (11)–(13) and then evaluating Eq. (15). The charged particle number densities, including charges on the aerosol particles, are obtained by solving Eqs. (11)–(13) and (15) iteratively in a self-consistent manner such that "f" in Eq. (14) is minimized.

For altitudes below 50 km, the mean free paths of electrons and positive ions become short relative to the sizes of the aerosols and embryos and the capture rates become diffusion dominated. To account for the changing situation, we use the approach of Rapp (2000) to calculate the capture rates. These results show that the mean charge on the largest particles (radius about 0.27 μm) at the surface is about 290, dropping with altitude to about 54 at 70 and 80 km and then rising as indicated in Fig. 6.

5.2. Evaluation of the terms in charge balance equations

5.2.1. Reaction rate constants

The values of the ionization rates Q have been discussed above. The positive ion–electron dissociative recombination coefficient α_1 is taken as 4.0×10^{-12} $m^3\,s^{-1}$ (Mitchell, 1990). This is a typical value for dissociative recombination coefficients for large positive ions (Banks and Kockarts, 1973). This coefficient is also used for the dissociative recombination of electrons with positively charged embryos.

α_2 is the pressure-dependent three-body recombination cross section for electrons with positive ions and positively charged embryos and is given by $\alpha_2 = 2 \times 10^{-37}(300/T)^{2.5} \times [N_2]$ $m^3\,s^{-1}$. It is important at low altitudes and is taken from Smith and Church (1977); here T is the absolute atmospheric temperature in K and N_2 is the nitrogen number density in m^{-3}. This three-body recombination coefficient is typical for electron–small-ion recombination in the presence of N_2. Its use significantly reduces the predicted electron abundance at altitudes below 100 km (see Fig. 3).

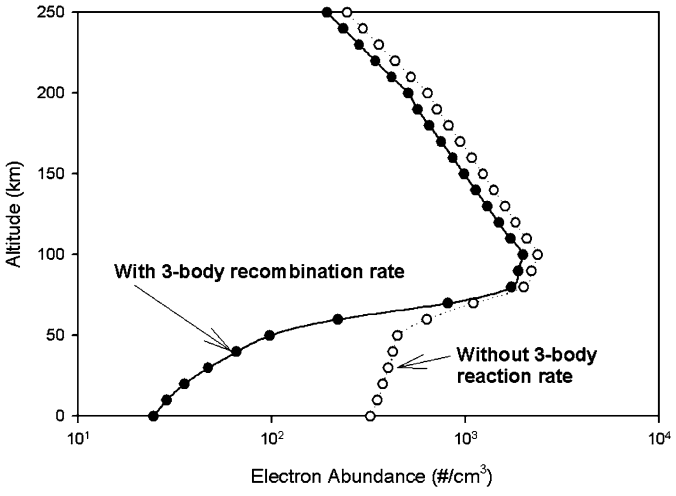

Fig. 3. Effect of including the three-body recombination rate on the predicted night time electron abundance for the assumption that no aerosols nor embryos are present.

α_3 is the negative ion–positive ion recombination coefficient (4.0×10^{-13} $m^3\,s^{-1}$). Such recombination coefficients are typically smaller than α_1 (for example, see Holland et al., 1977).

Attachment of electrons is taken from Bakes and Tielens (1994). Although the sticking coefficient may be very small when the electron affinity of a PAH molecule is less than 1 eV ($N_c < 25$–50; Allamandola et al., 1989), for simplicity, we adapted a value of unity, independent of PAH molecule size (Bakes and Tielens, 1994).

Ions are assumed to attach or discharge with unit probability upon collision with an aerosol particle. This assumption is reasonable because aerosol particles can accommodate charge more easily than molecular ions, which usually have relatively large ionization potentials and low electron affinities.

Because spacecraft measurements have not yet adequately determined the aerosol size distributions, abundances, nor their variation with altitude, the results of the theoretical model by Toon et al. (1992) are used to estimate these quantities. To verify that the chosen values of the bin size does not affect the results, two distribution of bins sizes were used:

(1) Narrow bins; here the bin limits were reduced by one-third, progressing from the upper limit of 0.31 μm; thus the lower limit of the largest bin was set at 0.2 μm, the next lower at 0.133, 0.0889, 0.059, 0.0395, and the lower limit of the final bin at 0.0263 μm.
(2) Wide bins; here the bin limits were reduced by one-half with the upper limit at 0.31 μm, followed by 0.15, 0.075, 0.038, 0.019, and 0.0095 μm.

The particle number density in each bin was obtained by adding the number of particles included in that bin from the much finer size distribution provided in the original data. The mean particle radius for each bin was obtained by computing the total volume of the particles in the bin and then calculating the mean radius r_i (or "mode") as follows: $r_i =$ (total volume of aerosols within bin limits/number density)$^{1/3}$, thus insuring conservation of mass. In each mode there are N_i aerosol particles per m^3.

5.2.2. Collisional charging of ions and aerosols

When calculating the loss of ions and electrons to aerosol particles, it is convenient to consider two collision regimes: the diffusion regime and the effusion regime. In the former, the mean free path between molecular collisions is short compared to the radius of the aerosol particle. In the latter, the mean free path is large compared to the aerosol radius.

In the effusion regime, the ion capture rates are based on Natanson (1960). (See also Jensen and Thomas, 1991.) The capture rate (m^3/s) of ions and electrons by neutral aerosols ($p = 0$) was calculated from

$$\nu_{p=0}^{i,j} = \pi r_i^2 \overline{v_j}\left[1 + \sqrt{\frac{e^2}{8\varepsilon_0 r_i kT}}\right], \tag{16}$$

where the "j" index covers captures by electrons, positive, and negative ions. The "i" index sums over all size bins. $\overline{v_j}$ is the

mean thermal velocity of the ion or electron, e is the elementary charge (coul), k is the Boltzmann constant, ε_0 is the permittivity of space, T is the temperature in K, and r_i is the radius of the aerosol particle in m. Equation (16) applies only to neutrally charged aerosols.

For charged aerosols ($p \neq 0$), the capture rate is more complex. At large distances, the Coulomb repulsive forces dominates for like charges but at small distances, the attractive image force dominates. For a particle with charge p, the distance at which the force changes from repulsive to attractive is set by a fifth-order algebraic equation

$$p = \frac{(2g^2 - 1)}{g(g^2 - 1)^2}, \tag{17a}$$

which is easily solved by the Newton–Raphson method. The attachment rate for charged aerosols in the effusive regime for the ith particle size mode is

$$\nu_{p\neq 0}^{ij} = \pi r_i^2 g^2 \overline{v_j} \exp\{-|p_i|c_i[1 - 1/2g|q|(g^2 - 1)]\}. \tag{17b}$$

Here p_i is the number of elementary charges (with sign) on aerosol particles of the ith size mode and

$$c_i = e^2/4\pi\varepsilon_0 r_i kT \quad \text{(dimensionless)}. \tag{17c}$$

At low altitudes where the mean free path is small compared to the particle size, we use a diffusion expression for the attachment rate

$$\nu_p^{i,j} = 4\pi r_i D^j H(i, j, p), \tag{18}$$

where $H(i, j, p)$ is a fit to the capture rate correction in Rapp (2000) (see his Fig. 56). D^e, D^+, and D^- are the positive ion, electron, and negative ion coefficients of diffusion ($m^2\,s^{-1}$), $j = 1, 2$, and 3, respectively.

Because the relative concentrations of molecular ions and electrons are so low compared to neutral molecules, the calculation of the loss of ions and electrons to aerosol particles were based on standard equations for diffusion and effusion with a simple geometrical summing that allows each process to dominate in the appropriate pressure/size range:

$$1/\nu_{\text{effective}} = 1/\nu_{\text{diffusion}} + 1/\nu_{\text{effusion}}, \tag{18e}$$

where the subscripts have been omitted for clarity. Note that the diffusion/effusion rate is controlled by the slower of the two expressions.

Next the loss rates are calculated:

$$d_e = \sum_{i,p} \nu_p^{i,1} N_{i,p}, \tag{19a}$$

$$d_+ = \sum_{i,p} \nu_p^{i,2} N_{i,p}, \tag{19b}$$

$$d_- = \sum_{i,p} \nu_p^{i,3} N_{i,p}, \tag{19c}$$

where "p" is the ion/electron charge index and "i" the size mode index and the ν refer to $\nu_{\text{effective}}$.

During the night, the aerosol charge occurs solely from the production of ions and electrons by electron precipitation and galactic cosmic ray bombardment. Because of the variations of ion and electron abundances and the gas density and temperature, the total charge accumulated by the aerosols also varies with height.

6. Effect of photoionization on aerosol charging

Calculations show that the reduction of solar flux due to aerosols still allows 1% to 3% of the flux at wavelengths longer than 210 nm to reach 50 km. Bakes et al. (2002) showed that this flux is sufficient to generate a high rate of photoionization and produce a substantial layer of ionization.

The photoelectric ejection rate ν_p in the radiation field of the Sun is given by the sum of the ejection rates for the negative ions and that for the aerosols

$$\nu_p = \int_{\lambda_{\min}}^{\lambda_{\max}} W(\lambda) f_{uv}(z, \lambda)[\sigma_x(\lambda)]\,\mathrm{d}\lambda \text{ electrons s}^{-1}, \tag{20}$$

where $W(\lambda)$ is the solar flux at Titan, $f_{uv}(z, \lambda)$ is the fraction of the incident solar flux present at altitude "z," σ_x is the cross section for photoproduction of electrons by negative ions and neutral aerosols, as appropriate. $\lambda_{\max}$ and $\lambda_{\min}$ define the wavelength range from the short wavelength cutoff due to CH_4 to the longest wavelength that produces photoionization. $\lambda_{\min}$ is approximately 155 nm whereas $\lambda_{\max}$ is a function of the aerosol size. Values for $\lambda_{\max}$ are listed in Table 3.

6.1. Attenuation of solar radiation by atmospheric absorption and scattering

The fraction of the incident solar flux present at altitude "z" includes the effects of Rayleigh scattering, molecular absorption by both major and minor species, and absorption and scattering by the aerosols.

Solar ultraviolet radiation responsible for ejecting electrons from the aerosol particles is attenuated in the Titan atmosphere via absorption by the aerosol particles and minor constituents such as acetylene, and by scattering from the aerosol particles and atmospheric molecules (mainly nitrogen). We have simulated this attenuation by the use of a two-stream radiative transfer model. By two stream we mean that the radiation directions are either downward or reciprocally upward through backscatter. (The mean solar zenith angle for the calculation is taken as

Table 3
Representative day time ionization potentials (in eV and nm)

	$k=-1$	$k=0$	$k=1$	$k=3$	$k=10$	$k=30$	$k=100$	$k=250$
Embryo	2.07	6.73	11.39					
(3 Å)	599	184	109					
Aerosol	4.33	4.47	4.61	4.89	5.87	8.66		
(0.01 μm)	287	278	269	254	211	143		
Aerosol	4.386	4.414	4.442	4.498	4.694	5.253	7.211	11.407
(0.05 μm)	283	281	279	276	264	236	172	109
Aerosol	4.39	4.41	4.42	4.45	4.55	4.83	5.81	7.903
(0.1 μm)	283	281	281	279	273	257	214	157

45°.) The two equations are (taken from Banks and Kockarts, 1973):

$$d\Phi^+/ds + \sum_i [\sigma_i^a + \sigma_i^s] n_i \Phi^+ = \sum_i n_i \sigma_i^s \Phi^-, \quad (21a)$$

$$d\Phi^-/ds - \sum_i [\sigma_i^a + \sigma_i^s] n_i \Phi^- = -\sum_i n_i \sigma_i^s \Phi^+, \quad (21b)$$

in which σ_i^a and σ_i^s are, respectively, the absorption and scattering cross sections of the ith species, n_i is the number density of the ith species, and $\Phi^+(\lambda, z)$ and $\Phi^-(\lambda, z)$ are, respectively, the downward and upward (scattered) solar ultraviolet intensities as functions of altitude, z and wavelength λ. The "z" direction is the slant distance as explained above. The intensities are taken in 0.01 μm intervals. The boundary conditions are $\Phi^+ =$ the unattenuated intensity (normalized to unity when no minor constituents are present) at 400 km altitude and $\Phi^- = 0$ at the planetary surface. When minor constituents are present, Φ^+ at 400 km altitude is reduced by the inclusion of a multiplicative factor

$$f = \exp\left(-\sum_i \sigma_i^a n_i H_i\right) \quad (22)$$

in which σ_i^a and n_i, H_i are now, respectively, the absorption cross section and the number density and the scale height of the ith species. The sums $\Phi^+(\lambda, z) + \Phi^-(\lambda, z)$ are thus the transmission coefficients that multiply the solar UV intensity in the photoemission subroutines at given altitude and wavelength. These coefficients are multiplied within the aerosol charging program by the solar UV intensities at each wavelength.

The computations are initiated by assuming that $\Phi^-(s) = 0$ at all altitudes with $\Phi^+(s)$ computed from the equation

$$d\Phi^+/ds + \sum_i [\sigma_i^a + \sigma_i^s] n_i \Phi^+ = 0. \quad (23)$$

The computations are then carried out iteratively with results from Eq. (23) substituted into Eq. (22) for the first iteration and so on. Convergence is rapid.

Absorption and scattering cross sections for the aerosol particles were computed by multiplying the geometric cross sections by the appropriate (wavelength-dependent) Mie coefficients (Draine, B.T., http://www.astro.princeton.edu/~draine/dust/dust.diel.html). The absorption cross sections of the minor constituents (e.g., acetylene) were supplied by (e.g., Kasting, J., 2003, private communication) while the mixing ratios were taken from Wilson and Atreya (2004). Scattering cross sections include Rayleigh scattering (computed using the results of Bates, 1984).

6.1.1. Absorption by minor constituents

Minor constituents known to be present in Titan's atmosphere and to have absorption bands at wavelengths longer than the CH_4 cutoff at 150 nm include C_2H_6, C_2H_2, C_2H_4, and HCN (Coustenis et al., 1991). Their abundance profiles for CH_4, C_2H_6, C_2H_2, C_2H_4, HCN, CH_3C_2H, HC_3N, C_4H_2, C_2N_2, CH_3CN were taken from the estimates of Wilson and Atreya (2004).

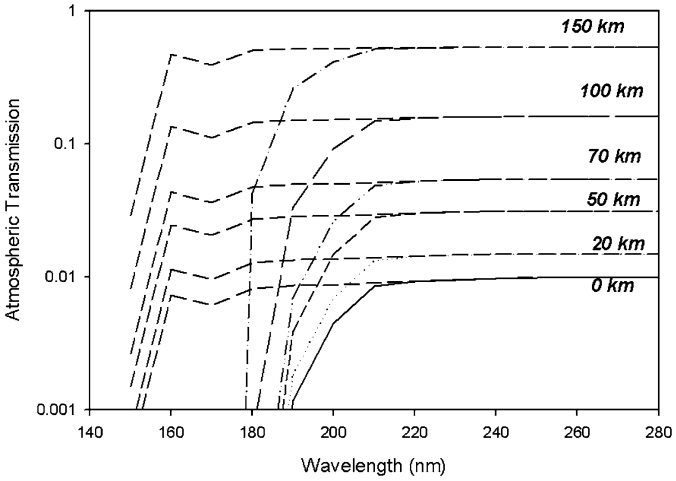

Fig. 4. Transmission as a function of wavelength for several altitudes. The dashed lines represent the situation when minor constituents are not present whereas the solid lines show the effects of their presence.

The presence of these minor constituents causes complete removal of the solar flux for wavelengths less than about 180 nm and substantial reductions in the flux at wavelengths as long as 200 nm. See Fig. 4.

6.2. The photoelectric ejection rate

The photoemission cross section is nonzero only for photons energetic enough to overcome the ionization potential (IP) of the aerosol particle. This ionization potential (Bakes and Tielens, 1994) is a function of particle radius and charge

$$IP = 4.4 + (Z + 0.5)^* 11.1/(N_c)^{1/3} \text{ (eV)}, \quad (24)$$

where N_c is the number of carbon atoms in the aerosol particle and Z is the particle charge. The first term on the RHS is the work function of graphite while the second term derived from the Coulomb potential term q/r. Because the particles are expected to be flattened rather than spherical, N_c is calculated from $N_c = 0.5r^3$, where r is in Å. Table 3 shows representative values of ionization potential for negative ions and aerosols.

The actual composition of the aerosols has not been determined and thus the ionization potential must be regarded as an estimate. See the excellent discussion in Bakes et al. (2002) about the composition of the molecules expected to comprise the smallest aerosols, i.e., embryos.

In order that minor constituents reduce the photoionization rate by a significant amount, the ionization potential must be sufficiently high that only the radiation in the UV portion of the spectrum, where the minor constituents have strong absorption bands, is effective in producing photoelectrons. Our model showed that because of the rapid increase in the solar flux with wavelength and the very low work function for the aerosols, attenuation by the minor constituents reduced the predicted electron abundances very slightly; i.e., about a 1% reduction at altitudes above 200 km. Similarly, only the charge states of the smallest aerosols and the embryo are affected by the reduced solar UV flux.

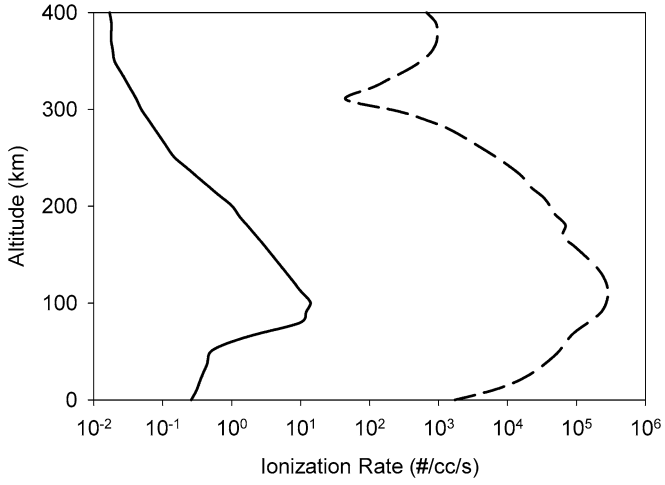

Fig. 5. Comparison of the photoionization rates due to GCR and photoemission from aerosols and negative ions. Solid curve is for ionization only by GCR. The dashed curve represents the photoemission from aerosols with a low ionization potential.

In Fig. 5, the photoionization rate is compared to that due to GCR. It is clear that the photoionization completely dominates the day time ionization rate for such low values of the ionization potential. This result implies that the day time and night time charge states of the aerosols will be quite different. The increase in the day time ionization rate above 300 km is due to the detached haze layer in Toon et al. (1992).

7. Results

7.1. Day time: Aerosol charging

To determine the effect of grouping the aerosols into finite width bins, the calculations were conducted with two sets of bin widths (refer to Section 5.2). To enhance the convergence of the calculations, only six bins were used for the calculations of the narrow bin distribution and only the five largest size bins for the "wide" case. Inclusion of the smallest size bin of the wide bins led to numerical convergence problems. This omission leads to very little error because the smallest size bin of the "wide" case carries little electrical charge.

A comparison was made for the predictions of the electron abundance versus altitude for the two methods of binning the aerosols. At most altitudes, the agreement was within 20%. The agreement is satisfactory given the large uncertainties in many of the parameters and implies that the predictions are generally not seriously affected by the choice of bin sizes.

Nevertheless, the calculations based on the use of wide bins generally predict slightly lower electron concentrations at all altitudes and significantly lower values at altitudes near 290 km. These differences are due to the fact that the wider bins cover a larger fraction of the total aerosol abundance than do the narrow bins. These additional aerosols provide additional surface area to reduce the electron abundance. Hence, unless stated otherwise, all the figures and tables are based on the use of the wide bins.

Figs. 6a–6e show that the peaks of the charge distributions move to larger values as the altitude increases. This variation is the result of the increased UV flux present at the highest altitudes. Clearly, the situation is quite different than that for the night where the peak of the distribution for a particular size changes slowly with altitude. The variation of the charge distribution for 0 km is quite different than that for the higher altitudes because at this altitude the aerosols are in the diffusion regime rather than the effusion regime. In the diffusion regime, the diffusion of the oppositely charged particles to neutralize charge is relatively slower than at higher altitudes.

Because of the low value of the aerosol ionization energy and the transparency of the atmosphere at high altitudes, the aerosols become very highly charged during the day time, of the order of 1500 charges per micron. This value is much larger than previously assumed in papers describing the formation of aerosols and is likely to substantially reduce the predicted thermal coagulation efficiency (Toon et al., 1992; Cabane et al., 1992, 1993). It should be noted that this result depends critically on the assumption that the ionization potential is low which in turn depends on the aerosol composition. For materials with higher ionization potentials, the day time charging levels will be lower and ultimately approach the night time levels if the potentials exceed 7.9 eV.

Fig. 7 shows that there is a large change in the fraction of embryos that are positively charged at low altitudes when the absorption due to minor constituents is considered. However, the absolute values of the abundances are insignificant.

As expected, the large abundance of free electrons reduces the abundance of positive ions to values substantially below that found in the reference case (where no aerosols or embryos are present). See Fig. 8.

7.2. Night time results: Ionization only by galactic cosmic rays (GCR)

Galactic cosmic rays (GCR) are the only source of ionization at night, yielding much smaller electron concentrations than in day time as shown in Fig. 9.

These results are somewhat qualitative since the relaxation times for capture of electrons by aerosol particles are long compared to the rotational period of Titan except for the largest particles. However, the relaxation times for capture of electrons by neutral embryos and the recombination times for negatively charged embryos with positive ions is very small (at most a few hours) compared to the rotation period. Hence the computed night time electron abundances should be approximately correct. A time-dependent model is required to obtain better estimates of the night time aerosol charge.

Fig. 10 presents a comparison of the electron and embryo abundances versus altitude. It is clear that the electron abundance is greatly reduced in the altitude range where the embryo abundance exceeds that of the electrons. In this region, the abundance of embryos is so large that the ionization rate by GCR is not sufficient to keep most of the embryos charged.

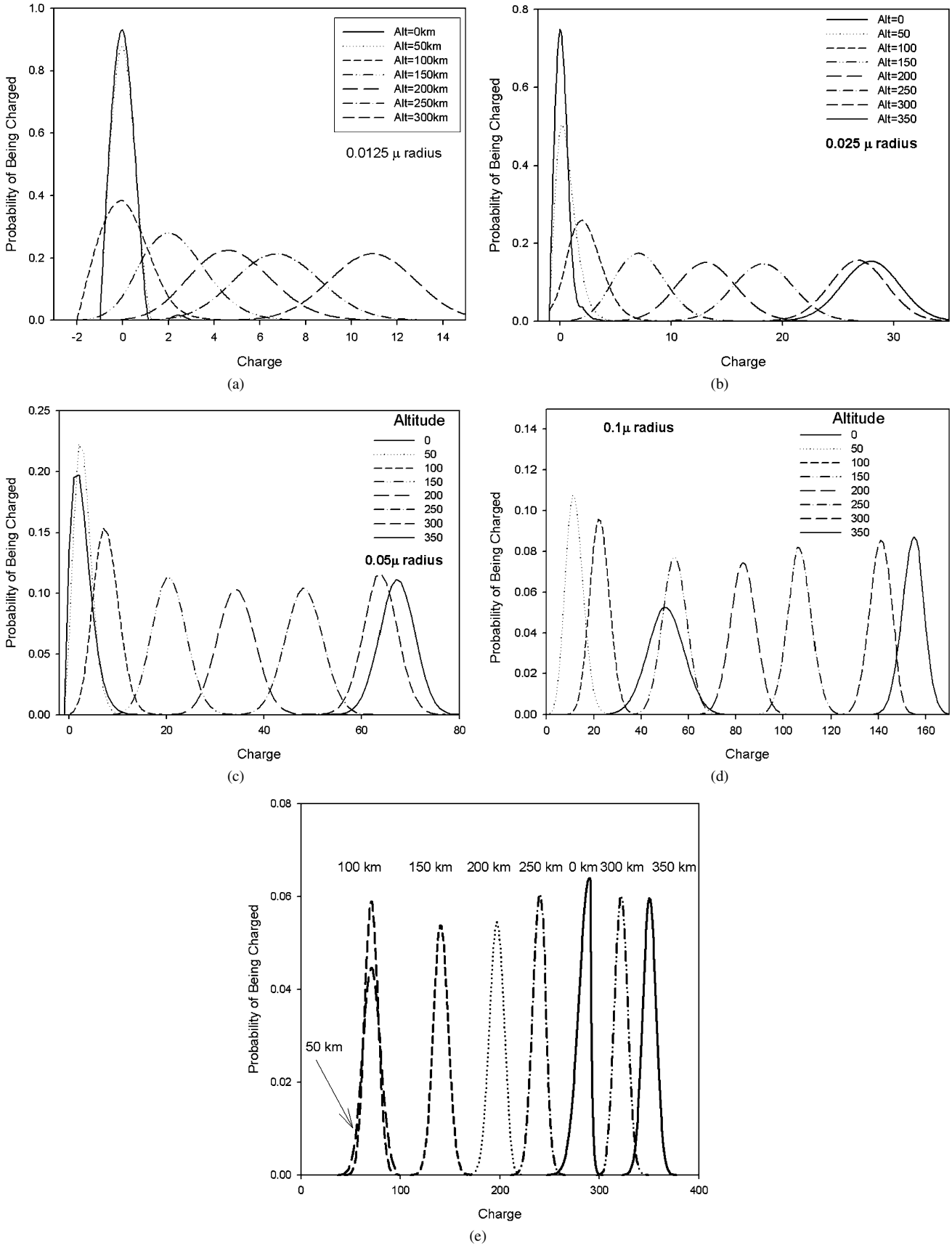

Fig. 6. (a) Day time charge distributions for ∼0.01 μm aerosols for various altitudes. (b) Day time charge distributions for ∼0.025 μm aerosols for various altitudes. (c) Day time charge distributions for ∼0.05 μm aerosols for various altitudes. (d) Day time charge distributions for ∼0.10 μm aerosols for various altitudes. (e) Day time charge distributions for ∼0.2 μm aerosols for various altitudes.

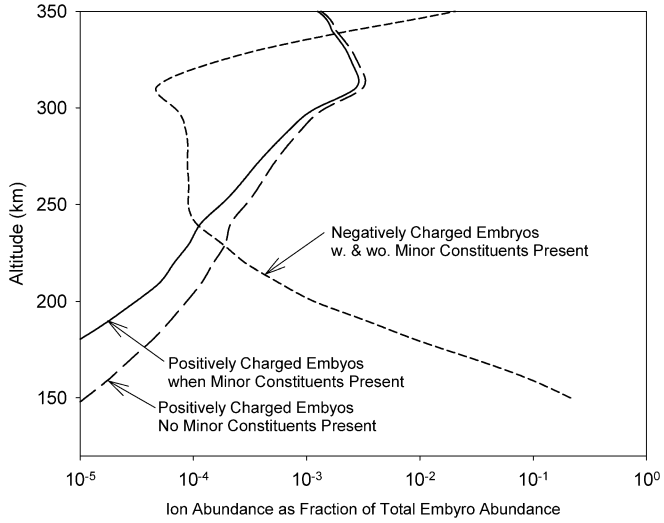

Fig. 7. Variation of the positively and negatively charged embryos with altitude.

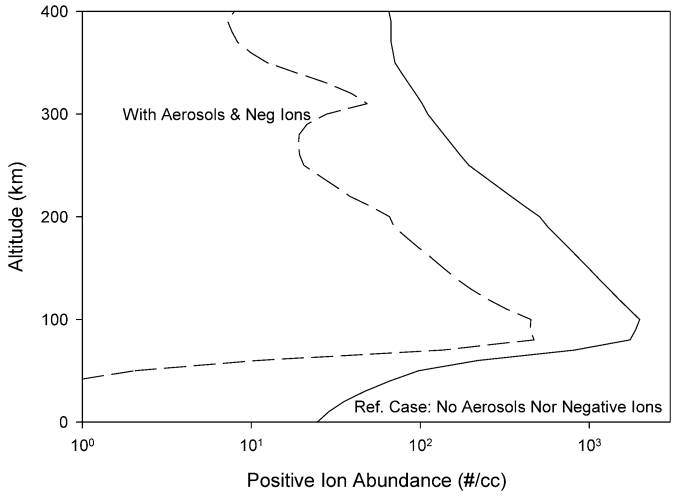

Fig. 8. Predicted day time positive ion abundances. Solid curve represents the reference case without aerosols and embryos. The dashed curve represents the situation when both are present.

7.3. Atmospheric conductivity calculations and comparison with the measurement capabilities of the plasma wave analyzer (PWA) on the Huygens Atmospheric Structure Instrument (HASI)[2]

Once the steady-state profiles of the ion and electron abundances and their mobilities have been determined, the scalar conductivity is calculated from the sum of the polar conductivities

$$\sigma = eK^e n^e + eK^+ n^+ + eK^- n^-. \tag{25}$$

At the time of Huygens Probe entry, the solar zenith angle should be between 35 and 65°. Hence we have calculated the conductivity for a solar zenith angle of 45°. The PWA should be operational from about 150 km to the surface. Fig. 11 shows that the predicted electron conductivity will be within the measurement range of the mutual impedance sensor below 90 km, but will exceed the measurement range above that altitude. The predicted positive ion conductivity shown in Fig. 12 should be in within the measurement range of the relaxation sensor down

[2] HASI Instrument parameters are taken from Fulchignoni et al. (2002).

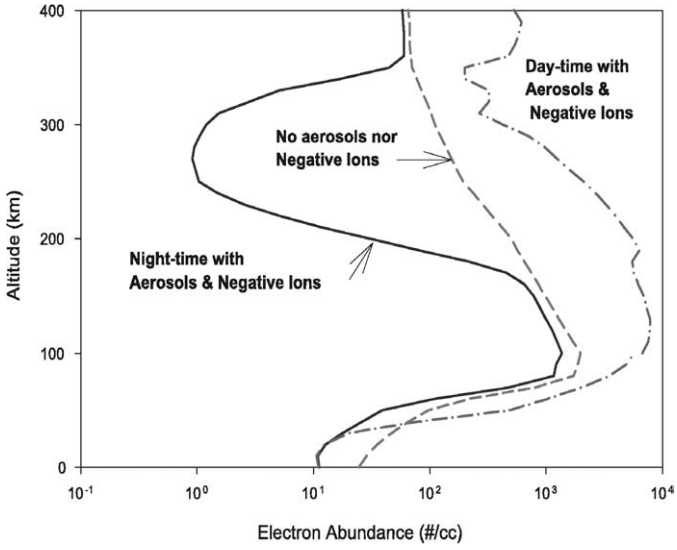

Fig. 9. Comparison of the predicted day- and night-time electron abundances with and without aerosols and negative ions.

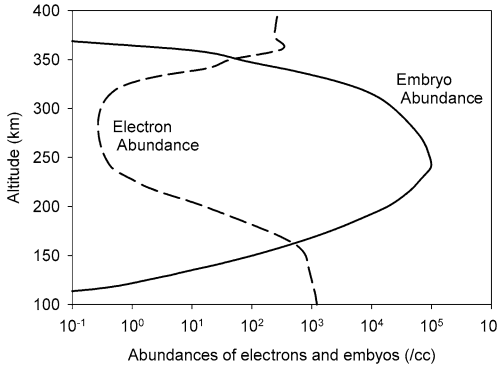

Fig. 10. Comparison of the night time abundance distributions of electrons and the embryos.

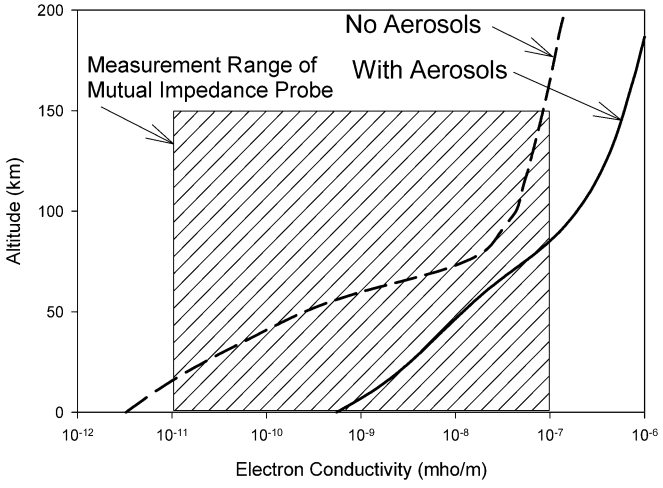

Fig. 11. Predictions for the electron conductivity in day time with aerosols and embryos (solid curve) and without either (dashed curve).

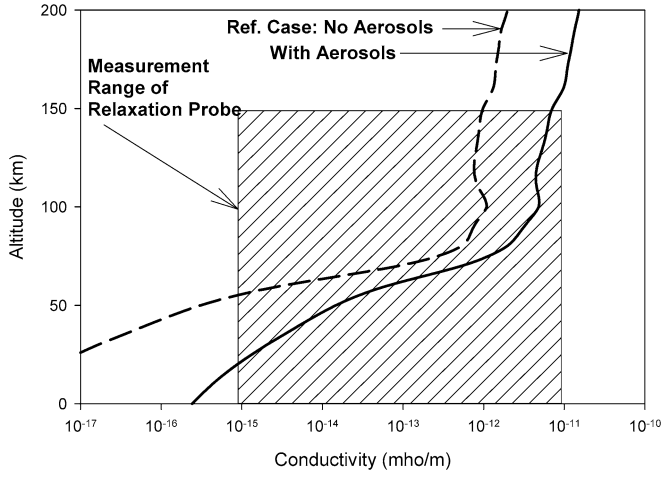

Fig. 12. Predictions for the positive ion conductivity in day time with aerosols and embryos (solid curve) and without either (dashed curve).

to an altitude of 50 km and then its abundance is expected to be too low to be detected. However, the predictions are strongly affected by the aerosol abundance and the low value for the ionization potential associated with the aerosol composition. If the abundance is lower or the *IP* is substantially higher than assumed here, then the predicted electron conductivity will be lower and the positive ion conductivity higher. In that case, the values of both parameters would be closer to the reference curves (solid lines) and could be within the instrument measurement capability over the entire altitude range.

Two other important parameters are the column aerosol density and the abundances of the minor constituents. Both influence the conductivity by regulating the amount of the solar flux available to produce photoionization.

It should also be noted that the predicted day time conductivity near the surface is approximately 10,000 times larger than terrestrial values (Rosen et al., 1982).

8. Relaxation times

In order to determine whether the charge on the aerosols on the dayside persists into the nightside, the characteristic relaxation time for each particle size mode was computed as a function of altitude. For characteristic times less than about 10^5 s,[3] the positive charges on the particles will be neutralized by electron capture before they are carried to the nightside. Table 4 shows that this was found to be the case.

Of greater interest with respect to the observable quantities are the characteristic times for electron loss to the (positively) charged aerosols. These times are shown in Table 5. The electron relaxation due to the presence of the aerosols is controlled by the largest aerosols. These times are sufficiently short during the day time that steady state computations simulate the electrical properties of Titan's atmosphere very well. At night, relaxation times are much longer so that a time dependent model is needed.

[3] The rotation period of Titan is 2.25×10^6 s.

Table 4
Relaxation times for aerosol charge versus altitude and particle size (day time conditions, s)

ALT/ size	0.0125 μm	0.025 μm	0.05 μm	0.1 μm	0.2 μm
0	0.8663E+01	0.1131E+01	0.9066E−01	0.2412E−01	0.1032E−01
50	0.2891E+01	0.2262E+00	0.3076E−01	0.5257E−02	0.1096E−02
100	0.3706E+00	0.5183E−01	0.9096E−02	0.1771E−02	0.3134E−03
150	0.1451E+00	0.2501E−01	0.4852E−02	0.9985E−03	0.2039E−03
200	0.1254E+00	0.2328E−01	0.2294E−02	0.4612E−03	0.2046E−03
250	0.2271E+00	0.4260E−01	0.8376E−02	0.1868E−02	0.2360E−03
300	0.7271E+00	0.1474E+00	0.3031E−01	0.7006E−02	0.1443E−02
350	0.7106E+00	0.1447E+00	0.2915E−01	0.6198E−02	0.1320E−02
400	0.4815E+00	0.9933E−01	0.2064E−01	0.4698E−02	0.8701E−03

Table 5
Relaxation times for electrons versus altitude and particle size (day time conditions, s)

ALT/ size	0.0125 μm	0.025 μm	0.05 μm	0.1 μm	0.2 μm
0	0.1247E+12	0.1628E+11	0.1377E+08	0.7910E+03	0.3041E+01
50	0.4667E+11	0.1386E+09	0.3434E+03	0.1154E+01	0.8632E−01
100	0.2208E+09	0.2347E+03	0.1118E+01	0.1042E+00	0.4547E−01
150	0.1057E+05	0.2184E+02	0.7785E+00	0.1236E+00	0.7118E−01
200	0.1497E+04	0.1991E+02	0.6604E+00	0.1262E+00	0.1708E+00
250	0.7818E+02	0.1015E+02	0.1881E+01	0.5831E+00	0.2735E+00
300	0.3029E+02	0.2050E+02	0.1089E+02	0.5572E+01	0.4442E+01
350	0.1379E+03	0.6907E+02	0.2428E+02	0.5048E+01	0.8025E+00
400	0.1356E+03	0.3103E+02	0.7312E+01	0.1916E+01	0.1072E+01

9. Conclusions

(1) The inclusion of the three-body recombination rate for electrons with positive ions substantially lowers the predicted electron abundance at low altitudes (and thereby, the conductivity) from that predicted by earlier models.
(2) Charging of aerosol particles has a major influence on both the electron abundance and electrical conductivity.
(3) For aerosol particles with low ionization potentials, the emission rate of photoelectrons on the dayside is so high that an ionosphere is created that greatly surpasses the one produced at night from the GCR bombardment.
(4) Our calculations for the dayside show that in the effusion regime above 50 km, the peaks of the charge distributions move to larger values as the altitude increases; at lower altitudes the situation is more complex.
(5) The distributions of charge on the aerosol particles show approximate agreement with those reported by Bakes et al. (2002). Differences are due to our simultaneous, self-consistent computation of electron and ion densities and charge distributions and our inclusion of a three-body recombination rate.
(6) During the day, the ratio of the charge to particle radius is very large, of the order of 1000 charges per micron. This value is much larger than previously assumed in papers describing the formation of aerosols and is likely to substantially reduce their thermal coagulation efficiency. At altitudes below ∼180 km and at night, the ratio of charge to particle radius is much smaller, typically 25 to 50 in quite

good agreement with the earlier results of Borucki et al. (1987). At altitudes in the range 180 to 350 km where the embryos are abundant, it is as small as ∼1 because of the reduced concentrations of electrons.

(7) Because of photodetachment of electrons from the negatively charged embryos as well as the migration of negative ions and their neutralization by the positively charged aerosol particles, the negative ion density on the dayside is substantially less than the electron density (i.e., of the order of 0.1). A small fraction of the embryos are positively charged as a result of photoemission of electrons.

(8) The predicted conductivities are within the measurement range of the HASI PWA instrument over much of the altitude range sampled. These predictions will need to be revised if the ionization potential of the aerosols is different than expected, or if the abundance distributions of the minor species or aerosols are different.

(9) Because the time constants electron relaxation at night are long compared to that of a Titan rotation period, a time-dependent model that considers the diurnal variation of the solar irradiation will be necessary to provide better estimates of the electrical state of Titan's atmosphere.

Acknowledgments

The authors thank Michel Cabane and Jean Lilensten for their help in reviewing the manuscript.

Appendix A

The ionization of methane and nitrogen by cosmic rays produces N_2^+, N^+, CH_4^+, CH_3^+, CH_2^+, H_2^+, and H^+. The nitrogenated cations, including N_3^+, N_4^+, created by molecular nitrogen association with N^+ and N_2^+, react with methane to increase the production of cations with one carbon. Therefore the charge transfer from N_4^+ to methane is the most important source for CH_4^+ below 200 km due to the very efficient reaction of tetranitrogen production in a nitrogen dominated atmosphere (Molina-Cuberos et al., 1999a). The direct ionization of methane by cosmic rays and the reaction

$$N^+ + CH_4 \rightarrow CH_4^+ + N \tag{R1}$$

are the main sources of CH_4^+ above 200 km.

The most abundant molecular species N_2, CH_4, and H_2 play an important role in the production of clusters with some of the ions and can act as an intermediate step in the CH_5^+ production. N_2 can cluster very efficiently with the ionized products of the methane dissociative ionization, CH_2^+ and CH_3^+, producing $CH_2^+\cdot(N_2)$, and $CH_5^+\cdot(N_2)$, respectively (Albritton, 1978) and shows an effective pathway for CH_5^+. The formation of the weakly bound cluster between CH_5^+ and CH_4 controls the loss processes of CH_5^+ in the troposphere. Dheandhanoo et al. (1984) measured the association and loss rates and found a coefficient of $8 \times 10^{-30}(300/T)^{3.5}$ cm^6 s^{-1} and $1.4 \times 10^{-8}(300/T)^{3.5}e^{-2230/T}$ cm^3 s^{-1}, respectively. At temperature higher than 75–80 K, that is, near the surface and above 60 km, the cluster destruction rate dominates due to exponential dependence of reverse reaction and clustering is not favored (Dheandhanoo et al., 1984).

Another cluster predicted in the atmosphere of Titan is $HCO^+\cdot H_2$. The protonated CO is produced by proton interchange between CH_5^+ and CO, with a rate coefficient of 9.9×10^{-10} cm^3 s^{-1} (Anicich and McEwan, 1997). This three-body-hydrogen clustering is very efficient because of the higher abundance of hydrogen than C_2 hydrocarbons. Earlier Capone et al. (1979, 1980) assumed that a new carbon bond will not be formed from the clustering of protonated saturated hydrocarbons such as CH_5^+ and $C_2H_7^+$ and assumed a rate coefficient of 10^{-29} to 10^{-31} cm^6 s^{-1}. But in new chemical scheme proposed by Molina-Cuberos et al. (1999a), $C_2H_7^+$ is produced from CH_5^+ via

$$CH_5^+ \xrightarrow{CO} HCO^+ \xrightarrow{C_2H_6} C_2H_7^+ \quad < 100 \text{ km}, \tag{R2}$$

$$CH_5^+ \xrightarrow{C_2H_6} C_2H_7^+ \quad > 100 \text{ km}. \tag{R3}$$

Bimolecular reaction of ethylene with $C_3H_5^+$ produces $C_5H_7^+$ and $C_5H_9^+$, with rate coefficients 1.2×10^{-10} and 5.11×10^{-11} cm^3 s^{-1}, respectively (Anicich and McEwan, 1997). Another cation $C_2H_5^+$ is mainly produced by methane reaction with CH_3^+ (Capone et al., 1980). Similar to protonated methane, methane can also cluster into protonated ethyl, resulting in $C_2H_5^+\cdot CH_4$.

In the lower atmosphere of Titan $HCNH^+$ plays very important role in the chemistry of nitrogenated ions (Molina-Cuberos et al., 1999a). In the model of Molina-Cuberos et al. (1999a), $HCNH^+$ is produced in a manner similar to that assumed by Capone et al. (1980):

$$N^+ \xrightarrow{N_2,M} N^{3+} \xrightarrow{CH_4} HCNH^+, \tag{R4}$$

$$N^+ \xrightarrow{CH_4} HCN^+ \xrightarrow{CH_4} HCNH^+. \tag{R5}$$

The reaction (R4) is very efficient in the production of $HCNH^+$ below 70 km while (R5) becomes important between 70 and 220 km. Above 220 km, $C_2H_5^+$ plays the most crucial role in the production of $HCNH^+$. Because of high proton affinity of the most abundant species in Titan, such as N_2, CH_4, H_2, and CO, $HCNH^+$ does not react with these by fast bimolecular processes. Instead only termolecular association involving acetylene, ethylene and HCN are favored in the high-density lower atmosphere:

$$HCNH^+ + C_2H_2 \xrightarrow{M} HCNH^+\bullet(C_2H_2)$$
$$5 \times 10^{-29} \text{ cm}^6 \text{ s}^{-1} \text{ (Anicich and McEwan, 1997)}, \tag{R6}$$

$$HCNH^+ + HCN \xrightarrow{M} HCNH^+\bullet HCN$$
$$5 \times 10^{-28}(300/T)^{3.9} \text{ cm}^6 \text{ s}^{-1}$$
$$\text{(Chatterjee and Johnsen, 1987)}, \tag{R7}$$

$$HCNH^+\bullet HCN + HCN \xrightarrow{M} HCNH^+\bullet(HCN)_2$$

$6.5 \times 10^{-28}(300/T)^{4.4}$ cm^6 s^{-1}

(Chatterjee and Johnsen, 1987). (R8)

It can be seen from this discussion that the high density and low temperature in the troposphere of Titan favor the association of methane with CH_5^+ and that $CH_5^+ \cdot CH_4$ is the most abundant cation from 15 to 65 km (Molina-Cuberos et al., 1999a). The high abundance of this ion is due to the efficiency of the methane cluster formation at the low temperatures of Titan's atmosphere. Below 15 km and between 65 and 80 km where $CH_5^+ \cdot CH_4$ is unstable, the CH_5^+ produces $HCO^+ \cdot (H_2)$. This process efficiently depletes most of the CH_5^+ making $HCO^+ \cdot (H_2)$ the most abundant cation from ground to 15 km and from 65 to 80 km. The dependence of the collisional destruction rate on temperature does not favor association at temperature greater than 75 or 80 K. The $CH_5^+ \cdot CH_4$ ion fraction profile is correlated with the thermal profile of the destruction rate. From 75 to 175 km, the most abundant cation is $C_7H_7^+$ produced from CH_5^+. Between 175 and 270 km, $C_4H_7^+$ is the most abundant cation produced by termolecular association of acetylene with $C_2H_5^+$ with a rate coefficient of 1.34×10^{-23} cm^6 s^{-1} (Burt et al., 1970). This coefficient is high enough for the formation of a covalent bond with an effective two-body coefficient higher than 10^{-25} cm^3 s^{-1} below 380 km (Molina-Cuberos et al., 1999a). The most abundant cation above 270 km is $H_4C_7N^+$, produced from diacetylene association with a high bimolecular rate coefficient of 8.7×10^{-10} cm^3 s^{-1}. The ion-mass versus altitude profile shown in Table 6 is based on these considerations.

Table 6
Calculated values of the mass of the ion clusters in Titan's atmosphere

Altitude (km)	Ion cluster	Current estimate of ion mass (amu)	Previous estimate of ion mass (amu)*
0	$HCO^+ \cdot H_2$	31	111
20	$CH_5^+ \cdot CH_4$	33	111
40	$CH_5^+ \cdot CH_4$	33	111
60	$CH_5^+ \cdot CH_4$	33	106
80	$HCO^+ \cdot H_2$	31	96
100	$C_7H_7^+$	31	83
120	$C_7H_7^+$	91	73
140	$C_7H_7^+$	91	63
160	$C_7H_7^+$	91	63
180	$C_7H_7^+$	55	78
200	$C_7H_7^+$	55	94
220	$C_7H_7^+$	55	109
240	$C_7H_7^+$	55	109
260	$C_7H_7^+$	55	109
280	$H_4C_7N^+$	102	109
300	$H_4C_7N^+$	102	109
320	$H_4C_7N^+$	102	108
340	$H_4C_7N^+$	102	104
360	$H_4C_7N^+$	102	101
380	$H_4C_7N^+$	102	97
400	$H_4C_7N^+$	102	93

* Borucki et al. (1987).

In our earlier model of the lower atmosphere (Borucki et al., 1987) $HCNH^+$ together with NH_4^+ were predicted to be the major ions, although they are mainly present in the form of clusters $NH_4^+ \cdot (NH_3)_n$ and $H_2CN^+ \cdot (HCN)_2$. Capone et al. (1980) argued that there may be sufficient ammonia in the lower atmosphere of Titan to allow to form NH_4^+ and the model of Borucki et al. (1987) was based on that assumption. The proton affinity of ammonia is higher than other species present in the Titan's atmosphere and therefore, if ammonia were present in sufficient quantity, that is with a mixing ratio greater than 2×10^{-6}, it would produce important amounts of $NH_4^+ \cdot (NH_3)_n$. However, ammonia has not been detected in the atmosphere (Molina-Cuberos et al., 1999b). Finally, we note that the termolecular ion–molecule association reactions of N_2 and CH_4 can play a greater role in Titan's lower atmosphere due to their concentrations being several orders of magnitude higher than other species (Milliagan et al., 2001).

Appendix B

The microphysics model (Toon et al., 1992; Barth and Toon, 2003) simulates the production, transport and growth of particles in a column of atmosphere. The particles are segregated into 35 bins that double in volume. Particles are created by unspecified photochemistry in the smallest bin with the function

$$q(z) = e^{-0.5((z-z_0)/z_s)^2}, \tag{B1}$$

where the scale height is $z_s = 25$ km and maximum mass production occurs at $z_0 = 250$ km. The profile is also adjusted so that only 3% of the mass production occurs above an altitude of 300 km.

The larger particle bins are populated through coagulation,

$$\frac{dn(a)}{dt} = 0.5 \int_0^a K_{\text{coag}}(a', a-a')n(a')n(a-a')\,da' - \int_0^\infty K_{\text{coag}}(a', a)n(a)n(a')\,da', \tag{B2}$$

where K is the coagulation kernel. The two terms in Eq. (B2) represent the creation of particles of size "a" through the coagulation of smaller particles and the loss of particles of size "a" as they coagulate to form larger particles, respectively. Brownian coagulation is the dominant coagulation process for tholin in Titan's atmosphere. The Brownian coagulation kernel is given by

$$K_{\text{Br}} = 2\pi(a_{p1} + a_{p2})(D_1 + D_2)b, \tag{B3}$$

where a_{pi} is the diameter of the ith particle and D_i is the diffusivity. The parameter b is a correction term for when the mean free path of the aerosol particle is comparable to the radius of the absorbing particle. In the continuum regime, $b = 1$ and the diffusivities can be represented by the Stokes–Einstein formula (where η is the atmospheric viscosity):

$$D_i = k_B T / 3\pi\eta a_{pi}. \quad \text{(B4)}$$

In Titan's atmosphere the particles are subject to charging below 300 km. This particle charging makes coagulation less efficient for small tholin particles. Transport is handled through sedimentation and eddy diffusion. The eddy diffusion coefficient varies with altitude as

$$K_{\text{diff}} = \begin{cases} 5000, & z \leqslant 90 \text{ km}, \\ 10^{((z+z1)/m)}, & 90 \text{ km} < z < 150 \text{ km}, \\ 2.5 \times 10^{13} n_{\text{gas}}^{-1/2}, & 150 \text{ km} \leqslant z < 400 \text{ km}, \\ 10^8, & z \geqslant 400 \text{ km}, \end{cases}$$

where $z1 = 95.471178$, $m = 50.141304$, n_{gas} is atmospheric number density, z is in km, and K_{diff} is in cm^2/s. Most particles are small enough to be controlled by eddy diffusion; sedimentation only applies to the largest few bins.

The final size distribution and aerosol profile were found by running the model to steady state, defined as the time when the mass flux of particles across the boundary of each 10 km layer matches the mass flux of particles out of the bottom of the model. Steady state was reached after a time of 500 years.

References

Allamandola, L.J., Tielens, A.G.G.M., Barker, J.R., 1989. Interstellar polycyclic aromatic hydrocarbons: The infrared emission bands, the excitation/emission mechanism, and the astrophysical implications. Astrophys. J. Suppl. 71, 733–775.

Albritton, D.L., 1978. Ion-neutral-rate constants measured in flow reactors through 1977. Atom. Nucl. Data Tables 22, 1–101.

Anicich, V.G., McEwan, M.J., 1997. Ion–molecule chemistry in Titan's ionosphere. Planet. Space Sci. 45, 897–921.

Bakes, E.L.O., Tielens, A.G.G.M., 1994. The photoelectric heating mechanism for very small graphitic grains and polycyclic aromatic hydrocarbons. Astrophys. J. 427, 822–838.

Bakes, E.L.O., Tielens, A.G.G.M., 1998. The effects of polycyclic aromatic hydrocarbons on the chemistry of photodissociation regions. Astrophys. J. 499, 258–266.

Bakes, E.L.O., McKay, C.P., Bauschlicher Jr., C.W., 2002. Photoelectric charging of submicron aerosols and macromolecules in the Titan haze. Icarus 157, 464–475.

Banks, P.M., Kockarts, G., 1973. Aeronomy, Part B. Academic Press, New York/London, pp. 257–260.

Barth, E.L., Toon, O.B., 2003. Microphysical modeling of ethane ice clouds in Titan's atmosphere. Icarus 162, 94–113.

Bates, D.R., 1984. Rayleigh scattering by air. Planet. Space Sci. 32 (6), 785–790.

Borucki, W.J., Levin, Z., Whitten, R.C., Keesee, R.G., Capone, L.A., Summers, A.L., Toon, O.B., Dubach, J., 1987. Predictions of the electrical conductivity and charging of the aerosols in Titan's atmosphere. Icarus 72, 604–622.

Burt, J.A., Dunn, J.L., McEwan, M.J., Sutton, M.M., Roche, A.E., Schiff, H.I., 1970. Some ion–molecular reactions of H_3^+ and the proton affinity of H_2^+. J. Chem. Phys. 52, 6062–6075.

Cabane, M., Chassefiere, E., Israel, G., 1992. Formation and growth of photochemical aerosols in Titan's atmosphere. Icarus 96, 176–189.

Cabane, M., Rannou, P., Chassefiere, E., Israel, G., 1993. Fractal aggregates in Titan's atmosphere. Planet. Space Sci. 41, 257–267.

Capone, L.A., Dubach, J., Whitten, R.C., Prasad, S.S., 1979. Cosmic ray ionization of the jovian atmosphere. Icarus 39, 433–449.

Capone, L.A., Dubach, J., Whitten, R.C., Prasad, S.S., 1980. Cosmic ray synthesis of organic molecules in Titan's atmosphere. Icarus 44, 72–84.

Chatterjee, B.K., Johnsen, R., 1987. Clustering reactions of H_2CN^+ ions with HCN. J. Chem. Phys. 87, 2399–2400.

Coustenis, A., Bézard, B., Gautier, D., Marten, A., 1991. Titan's atmosphere from Voyager infrared observations. Icarus 89, 152–167.

Coustenis, A., Salama, A., Schulz, B., Ott, S., Lellouch, E., Encrenaz, Th., Gautier, D., Feuchtgruber, H., 2003. Titan's atmosphere from ISO mid-infrared spectroscopy. Icarus 161, 383–403.

Dheandhanoo, S., Johnsen, R., Biondi, M.A., 1984. Measured ion–molecule reaction rates for modeling Titan's atmosphere. Planet. Space Sci. 32, 1301–1305.

Fulchignoni, M., and 27 colleagues, 2002. The characterization of Titan's atmospheric physical properties by the Huygens Atmospheric Structure Instrument (HASI). Space Sci. Rev. 104, 395–431.

Hodges, R.R., 1969. Ion pair annihilation by aerosols in the lower ionosphere. J. Geophys. Res. 74, 2223–2228.

Holland, D.H., Archer, D.H., Berkowitz, J.J., Hart, W.C., Hendrick, R.W., Humphrey, C., 1977. Physics of high altitude nuclear burst effects. Defense Nuclear Agency. Final Report, Contract DNA 001-73-C-0102.

Hu, H., Holzworth, R.H., 1996. Observation and parameterization of the stratospheric electrical conductivity. J. Geophys. Res. 101, 29539–29552.

Jensen, E.J., Thomas, G.E., 1991. Charging mesospheric particles: Implications for electron density and particle coagulation. J. Geophys. Res. 96 (D10), 18603–18615.

Kilpatric, W.D., 1971. An experimental mass-mobility relation for ions in air at atmospheric pressure. Proc. Annu. Conf. Mass Spectrosc. 19, 320–325.

Krimingis, S.M., Carbary, J.F., Keath, E.P., Armstrong, T.P., Lanzerotti, L.J., Gloeckler, G., 1983. General characteristics of hot plasma and energetic particles in the saturnian magnetosphere: Results for Voyager spacecraft. J. Geophys. Res. 88, 8871–8892.

Landau, L.D., Lifshitz, E.M., Pitaevskii, L.P., 1984. Electrodynamics of Continuous Media, second ed. Pergamon Press, New York, pp. 8–10.

Lara, L.M., Lellouch, E., Lopez-Moreno, J.J., Rodrigo, R.J., 1996. Vertical distribution of Titan's atmospheric constituents. J. Geophys. Res. 101, 23261–23283.

Lara, L.M., Lelloch, E., Shematovich, V., 1999. Titan's atmospheric haze: The case for HCN incorporation. Astron. Astrophys. 341, 312–317.

Lebonnois, S., Bakes, E.L.O., McKay, C.P., 2002. Transition from gaseous compounds to aerosols in Titan's atmosphere. Icarus 159, 505–517.

McDaniel, E.W., Mason, E.A., 1973. The Mobility and Diffusion of Ions in Gases. Wiley, New York.

Meyerott, R.E., Reagan, J.B., Joiner, R.G., 1980. The mobility and concentration of ions and the ionic conductivity in the lower ionosphere. J. Geophys. Res. 85, 1273–1278.

Milliagan, D.B., Freeman, C.G., MaClagan, R.G.A.R., McEvan, M.J., Wilson, P.F., Anicich, V.G., 2001. Termolecular ion–molecule reactions in Titan's atmosphere. II. The structure of the association adducts of $HCNH^+$ with C_2H_2 and C_2H_4. J. Am. Soc. Mass Spectr. 2, 557–564.

Mitchell, J.B.A., 1990. The dissociative recombination of molecular ions. Phys. Rep. 186, 215–248.

Molina-Cuberos, G.J., Lopez-Moreno, J.J., Rodrigo, R., Lara, L.M., 1999a. Chemistry of the galactic cosmic ray induced ionosphere of Titan. J. Geophys. Res. 104, 21997–22024.

Molina-Cuberos, G.J., Lopez-Moreno, J.J., Rodrigo, R., Lara, L.M., O'Brien, K., 1999b. Ionization by cosmic rays of the atmosphere of Titan. Planet. Space Sci. 47, 1347–1354.

Molina-Cuberos, G.J., Lopez-Moreno, J.J., Rodrigo, R., Lara, L.M., 2000. Influence of electrophilic species on the lower atmosphere of Titan. Geophys. Res. Lett. 27, 1351–1354.

Natanson, G.L., 1960. On the theory of the charging of amicroscopic aerosol particles as a result of capture of gas ions. Zh. Tekh. Fiz. 30, 573–588 (English transl. Soviet Phys. Tech. Phys. 5, 538–551).

Nelder, J.A., Mead, R., 1965. A simplex method for function minimization. Comput. J. 7, 308–313.

O'Brien, K., 1970. Calculated cosmic ray ionization in the lower ionosphere. J. Geophys. Res. 75, 4357–4359.

O'Brien, K., 1971. Cosmic-ray ionization in the atmosphere. Nuovo Cimento A 3, 521–547.

O'Brien, K., 1972. Propagation of muons underground and the primary cosmic-ray spectrum below 40 TeV. Phys. Rev. D 5, 597–605.

O'Brien, K., 1975a. The cosmic ray field at ground level. In: Natural Radiation Environment. II. USERDA Rep. CONF-72085. Part 1. U.S. Department of Commerce, National Technical Information Service, Springfield, VA, pp. 15–54.

O'Brien, K., 1975b. Calculated cosmic-ray pion and proton fluxes at sea level. J. Phys. A 8, 1530–1534.

Parthasarathty, R., 1976. Mesopause dust as a sink for ionization. J. Geophys. Res. 81, 2392–2396.

Press, W.H., Flannery, B.P., Teukolosky, S.A., Vetterling, W.T., 1986. Numerical Recipes. Cambridge Univ. Press, Cambridge, UK. Chap. 10, Section 4, Downhill simplex method in multidimensions.

Rages, K., Pollack, J.B., Smith, P.H., 1983. Size estimates of Titan's aerosols based on Voyager high-phase angle images. J. Geophys. Res. 88, 8721–8728.

Rages, K., Pollack, J.B., 1983. Vertical distribution of scattering hazes in Titan's upper atmosphere. Icarus 55, 50–62.

Ramanan, G., Freeman, G.R., 1990. Electron mobilities in low density helium and nitrogen gases: Momentum transfer cross sections at very low energies. J. Chem. Phys. 93 (5), 3120–3125.

Rannou, P., Carbane, M., Chassefiere, E., Botet, R., McKay, C.P., Courtin, R., 1995. Titan's geometrical albedo: Role of the fractal structure of the aerosols. Icarus 118, 355–372.

Rannou, P., Carbane, M., Botet, R., Chassefiere, E., 1997. A new interpretation of scattered light measurements at Titan's limb. J. Geophys. Res. (Earth) 102, 10997–11013.

Rapp, M., 2000. Aerosol layers in the polar mesosphere. Interaction with the plasm of the D-region and dependence on temperature. Report BONN-IR-2000-02. University of Bonn, FRG.

Rosen, J.M., Hoffman, D.J., Gringel, W., Berlinski, J., Michrowsky, S., Morita, Y., Ogawa, T., Olsen, D.J., 1982. Results of an international workshop on atmospheric electrical measurements. J. Geophys. Res. 87, 1219–1227.

Smith, D., Church, M.J., 1977. Ion–ion recombination rates in the Earth's atmosphere. Planet. Space Sci. 25, 433–439.

Tomasko, M.G., Smith, P.H., 1982. Photometry and polarimetry of Titan: Pioneer 11 observations and their implication for aerosol properties. Icarus 51, 65–95.

Toon, O.B., McKay, C.P., Griffith, C.A., Turco, R.P., 1992. A physical model of Titan's aerosols. Icarus 95, 24–53.

Vogt, R.E., Chenette, D.L., Cummings, A.C., Garrard, T.L., Stone, E.C., Schardt, A.W., Trainor, J.H., Lal, N., McDonald, F.B., 1981. Energetic charged particles in Saturn's magnetosphere: Voyager 1 results. Science 212, 231–234.

West, R.A., Lane, A.L., Hart, H., Simmons, K.E., Hord, C.W., Coffeen, D.L., Esposito, L.W., Sato, M., Pomphrey, R.B., 1983. Voyager 2 photopolarimeter observations of Titan. J. Geophys. Res. 88, 8699–8708.

Wilson, E.H., Atreya, S.K., 2004. Current state of modeling the photochemistry of Titan's mutually dependent atmosphere and ionosphere. J. Geophys. Res. (Planets) 109, doi:10.1029/2003JE002181. E06002.

Yelle, R.V., Strobell, D.F., Lellouch, E., Gautier, D., 1996. Engineering Models for Titan's Atmosphere. ESA Publ. SP-1177. ESA Publications Division, Noordwijk, pp. 243–256.